Pergamon

Journal of Structural Geology, Vol. 18, No. 5, pp. 673 to 687, 1996

0191-8141/96 $15.00+0.00

0191-8141(95)00105-0

Experimental modeling of extensional fault systems by use of plaster

HAAKON FOSSEN

Statoil, N-5020 Bergen, Norway

and

ROY H. GABRIELSEN

Geologisk Institutt, Universitetet i Bergen, Allégt. 41, N-5007 Bergen, Norway

(*Received* 24 *November* 1994; *accepted in revised form* 22 *August* 1995)

Abstract—Plane-strain extension experiments with plaster as the deforming medium produce faults and related structures that closely resemble natural examples. The faults with the largest displacement are normally developed at about 25% overall extension ($\beta = 1.25$). Major faults develop as composite structures, and although the main movement may be accommodated by a relatively simple slip surface, the fault zones commonly develop internal, lense-shaped geometries. Small, synthetic faults dipping more steeply than the main zone are typical components of the fault zones, particularly on the hanging wall side. Fault displacements develop over 2 orders of magnitude, and the distribution of fault displacements closely follows a power-law relationship similar to data from seismic and field mapping.

The main, through-cutting faults accommodate about 60–70% of the total deformation, while smaller, visible faults typically account for *ca* 10–20%. Only 20–30% extension is due to faults and ductile deformation that occur below the resolution of the models, which roughly corresponds to seismic resolution when scaled up to natural size. The internal fault-block formation may include zones of normal faults accommodating significant internal shear deformation associated with collapse of fault blocks. Collapse has been recorded in the upper part of footwalls, resulting in a flattening of the upper part of the main faults.

Although internal block deformation by simple shear or other deformations can be shown to play a significant role in the deformation, a component of rigid-block rotation is demonstrated, for example by the rotation of steep normal faults into orientations where they appear as reverse faults. Copyright © 1996 Elsevier Science Ltd

INTRODUCTION

The techniques of physical model studies in structural geology are not at all new (e.g. Cadel 1890), and clay experiments were extensively used by Cloos (1929, 1930, 1931), and later by Rettger (1935), Cloos (1955, 1968) and Tchalenko (1970). Challenges in exploration for and exploitation of oil and gas have recently emphasized the need for detailed understanding of development and geometries of hydrocarbon traps. Such demands have been met with the development of miscellaneous computer modeling tools, but has also generated a renewed interest in scaled analog models, with emphasis on the analysis of extensional faults.

In most previously published experimental studies of faulting, clay (H. Cloos, 1929, 1930, E. Cloos 1955, 1968, Oertel 1962, 1965, Withjack *et al.* 1995) or sand (e.g. Horsfield 1977, 1980, McClay & Ellis 1987a,b, Mandl 1988, McClay 1990, Braun *et al.* 1994) have been used as modeling material, either alone or in combination with less common materials such as silicone putty and honey (Vendeville *et al.* 1987, Brun *et al.* 1994). These materials are well suited for analysis of fault processes, but may be hampered by their inabilities to develop and preserve the most delicate fault structures. To improve modeling in this respect, Sales (1987) designed a method to apply soft plaster as the modeling material. Because of its very fine grain size, its fast transition from liquid to solid state, and its durability after solidification, plaster experiments produce extremely detailed models which may be preserved and studied in detail at any time. A number of experiments with plaster have been run at the Structural Geology Laboratory, Geological Institute, University of Bergen. Detailed analysis of these plaster models have greatly contributed to an understanding of geometrical principles in fault analysis (Odinsen 1992) and of regional problems (Grunnaleite 1991, Ottesen 1991, Gabrielsen *et al.* 1992).

The present study was designed to investigate the development, geometry and kinematics or transport of fault blocks in pure extension and to study the development of small-scale structures in relation to larger fault systems.

SCALING, EXPERIMENTAL DESIGN AND PROCEDURE

Physical constraints for use of materials and scaling of models in structural geology were originally set by Hubbert (1937), and theoretical aspects of scaled modeling were further investigated by Ramberg (1981). These works serve as a base for most later, scaled analogue models. Sales (1987) made clear that it is not possible to arrange a tectonic model truly dynamically similar to a

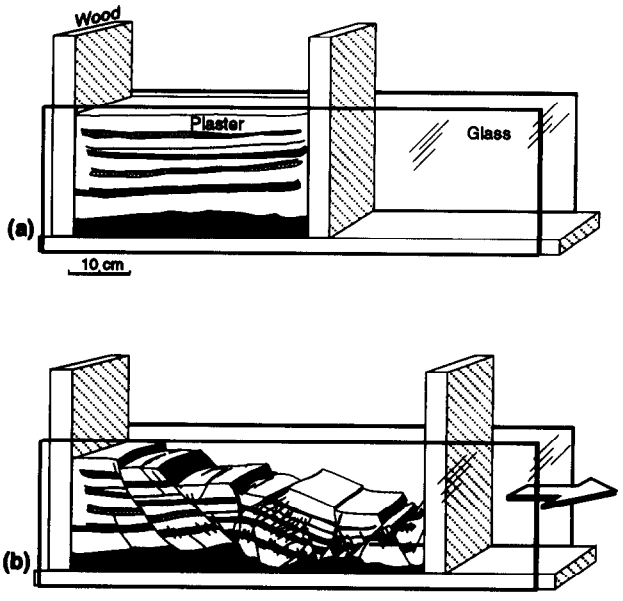

Fig. 1. Illustration of the deformation rig used in the plaster experiments. During the runs the moveable wood wall was moved to the right to create a plane-strain (extensional) deformation.

natural example. Problems arise from our limited knowledge of rheological properties of rocks, scarceness of rheologically appropriate materials, complications involved in sectioning the weak, rheologically correct materials that may exist, and problems with time–length relationships, but Sales' experience with plaster (with or without barite at the base of the model) suggests that at least some of these problems can be overcome or neglected for plaster models. Sales (1987) discussed the consequences of scaling for plaster models in detail. The present experiments have been prepared with the North Sea and similar extensional basins in mind, and the scaling factor is *ca* 10^{-4}–10^{-5} for the northern North Sea area, i.e. 1 cm in the model represents 0.1–1 km in nature.

Plaster models have the advantage that they can be run with unsophisticated equipment and with a variety of set-ups. In the present study, a simple box with a fixed, flat wooden base, two fixed glass walls and two short wooden walls (one fixed and one moveable) was used (Fig. 1). The upper surface is unconstrained, and corresponds to the surface of the earth in natural analogs. The walls were sealed with sheet rubber, and the box was tightened by rubber bands. Following the procedure described by Sales (1987), the walls were lubricated with oil, and markers (stripes of carbon powder) were painted on the sides of the plaster model with a laboratory brush. The stripes mimic a non-mechanical, sedimentary layering that deforms perfectly along with the plaster. Unlike some previous experiments (e.g. Ellis & McClay 1988) we do not use a controlling basement fault or fixed footwall geometry to study hanging wall deformation, but merely apply plane-strain extension to a volume of plaster and barite to study the extensional structures that develop.

A soft, wet barite mass was placed at the base of the experiment to create a basement relief, and the moveable short wall was moved by hand away from the fixed short wall. During this movement, the plaster collapses under its own weight, and a series of extensional structures are produced which can be studied through the glass wall during the experiment, and in more detail when the plaster has solidified (Fig. 2a). If the upper, free surface had remained horizontal throughout the experiment, the bulk deformation would have been perfect pure shear.

The plaster is pored into the box when liquid and, accordingly, no mechanical layering exists within the model. Since the short wall is retracted by hand, the strain rate is not constant during the experiment. This non-steady strain rate is necessary to keep pace with the rapid solidification process and may in fact be consistent with what actually happens along seismogenic faults. Typical runs are performed with varying strain rate within a period of 60–120 s.

The deformation was recorded using a video camera and still photography. Black and white drawings from intermediate stages were made from the photographs and video recordings. These drawings were used for studies of fault development, block rotations, strain and particle paths during deformation. Detailed drawings of the final stage of the plaster experiments were made on transparent paper placed directly on the solidified plaster.

Plaster as an experimental medium—advantages and limitations

Plaster experiments are easily arranged and performed once some experience has been gained. On the other hand, certain problems cannot be avoided. One complicating factor typical of plaster experiments is that the gradual solidification and expulsion of water cause changes in the physical conditions of the plaster during the course of the experiment. It is not easy to quantify these temporally changing conditions, and hence the rheological scaling problem is less controllable than for sand-box experiments. One way of approaching this problem is to study the initial angle of failure in plaster. If the physical properties of the plaster change, i.e. if the angle of internal friction changes, then the initial angle of faulting (θ) should change also. This relationship was exploited to some extent by studying in detail the initial angle of faulting during one of the experiments presented in this paper (run 2, see later). The mean value of θ for new faults for various strain increments is presented in Fig. 3. Although the resolution of the data is limited, it appears that θ varies a small amount during the experiment. Statistically, there is a tendency for θ to decrease towards the end of the experiment, although the presence of a large fault population at this stage may obscure the implication of this observation. Assuming that the simple relationship between the coefficient of internal friction (μ) and θ holds, i.e. that

$$\mu = \tan (20 - 90°)$$

(assuming that σ_1 is vertical), μ can be calculated to

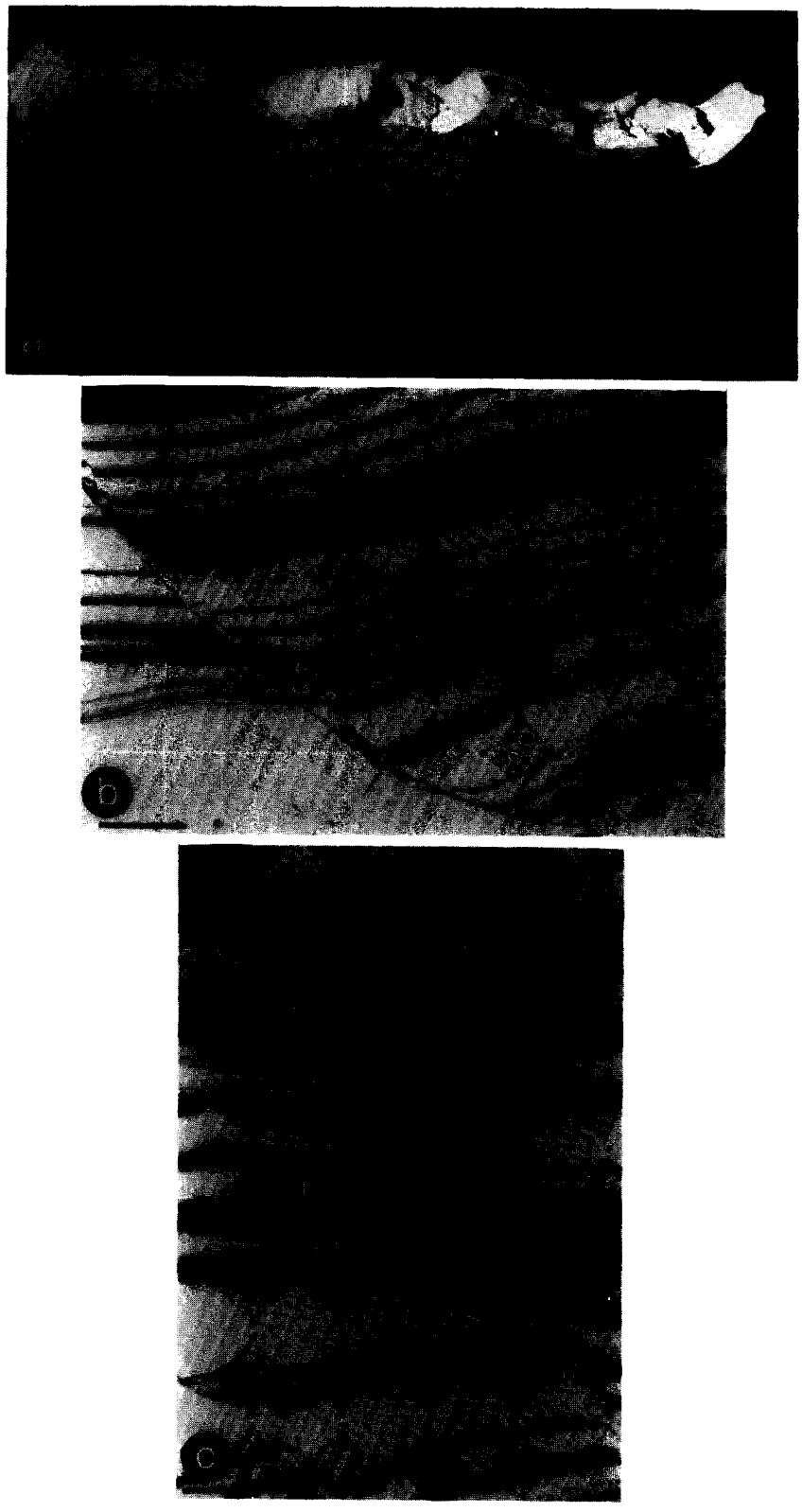

Fig. 2. (a) Photograph of final result of run 2 after the glass walls have been removed. Length of the deformed block is 60 cm. (b) Photograph of fault 3, run 1, showing the typical association of parasitic, small faults and the main fault plane illustrated in Fig. 11(a). Scale bar = 2 cm. (c) Combination of the two types of fault morphologies illustrated in Fig. 11, i.e. fault-bounded lensoidal structures and steeper faults that are connected to the main fault and die out into the hanging wall (or footwall). Fault 1, run 1 (see Fig. 6d for fault numbers). Scale bar = 2 cm.

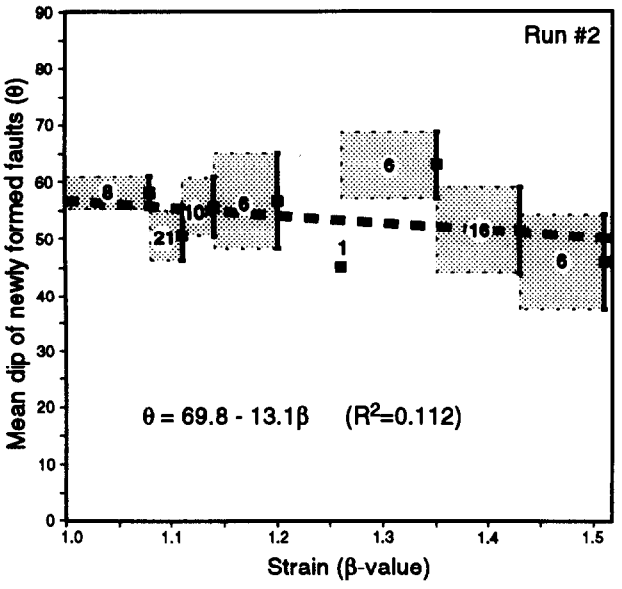

Fig. 3. Dip of new faults developed during eight successive strain increments during run 2. Error bars indicate the standard deviation of each group of data. Numbers in boxes show the number of faults recorded during each strain increment. A linear regression is fitted to the data, and the corresponding formula is displayed. The data were collected by measuring fault dips from line drawings of slides shot during the experiment. β is the extension factor.

approximately 0.45 in early and intermediate stages of the experiment. The value of μ may be higher in natural rocks, commonly between 0.6 and 0.8 (Byerlee 1978), and natural faults accordingly tend to initiate with somewhat steeper dips than the ones observed in plaster experiments (see Walsh & Watterson 1988 and references therein).

The cohesive strength of natural rocks is neglected in sand-box experiments, where dry, cohesionless sand is normally used. In contrast, plaster (and clay) experiments exhibit cohesive strengths that are too high when scaled up to natural scale. Also, the short duration of plaster or clay experiments does not allow water to drain out rapidly enough to prevent a component of ductile deformation before faulting is initiated (cf. Naylor *et al.* 1986). In the experiments discussed in this paper, about 5–10% ductile extension is recorded prior to faulting.

The mechanical scaling problem of plaster is compensated by some advantages of the medium. The large grain size in sand is not to scale in sand-box experiments, and results in unrealistically wide (thick) shear zones. Faults in plaster models appear, however, to be narrower and thus more similar to their natural counterparts due to a uniform fine grain size. Furthermore, two orders of faults develop in plaster experiments, whereas in sand experiments, only one order of faults is normally developed in full. The wide range in fault size in plaster models makes it possible to study the relation between main faults and associated minor faulting in a unique way. The fact that there is no real, physical layering in the plaster models means that the deforming medium has almost isotropic mechanical properties (although a water pressure gradient may have an effect in the vertical direction). Therefore, no bedding-parallel slip (flexural-slip) mechanism is preferentially developed, and internal block deformation must occur by some other mechanism.

Perhaps the best argument for using plaster models as a complimentary method to sand-box and other model types is simply that the resulting structures are so remarkably similar to these observed in naturally extended crust (Fig. 4). Although the general geometries may be equally well produced by, for instance, sand experiments (cf. Figs. 4a & b), the opportunity to study associated small-scale deformation is so far unique to plaster experiments. We therefore believe that plaster experiments, although not as well constrained as some other media, provide important additional information about extensional crustal deformation.

RESULTS

Three plane-strain extensional experiments, in which the plaster had similar rheological properties, but slightly different boundary conditions, were successfully performed. Run 1 was prepared with a relatively stiff (viscous) basement (wet barite). Run 2 is similar to run 1, but the basement was less viscous (higher water content), so that it should deform along with the overlying plaster. The third run also had an easily flowing barite basement, and pre-cut aluminum plates were placed between the plaster and the barite basement to control the deformation (see below). The end results of these three experiments are shown in Figs. 5(a)–(c) (a photograph of the final stage of run 2 is shown in Fig. 2a).

Observations—Run 1 (stiff basement)

The relatively stiff (viscous) barite basement in this run resulted in the development of an extensional ramp geometry early in the experiment. Because the active barite basement only underwent a very small amount of deformation, a décollement with increasing displacement to the right developed between the barite basement and the plaster. The first main fault (1 in Fig. 6) developed above the ramp. Fault 1 was passively transported away from the ramp as subsequent synthetic faults formed in the footwall to fault 1 (Figs. 6b & c).

Four main fault blocks (A–D in Fig. 6d) formed as faulting migrated into the footwall of the first fault. In contrast to the earlier main faults, the third fault (3 in Fig. 6) gradually developed a listric shape and soles out above the basement to the left of the ramp zone. Consequently, a part of block C and fault 2 were rotated and deformed (Figs. 6d–g). It should also be noted that fault 3 developed its listric geometry during the course of the experiment. Obviously, this means that block D underwent some internal deformation below the scale of visual resolution, although not as much as block C. During these first stages of the experiment, the early faults were passively transported to the right, whereas the area of faulting expanded to the left.

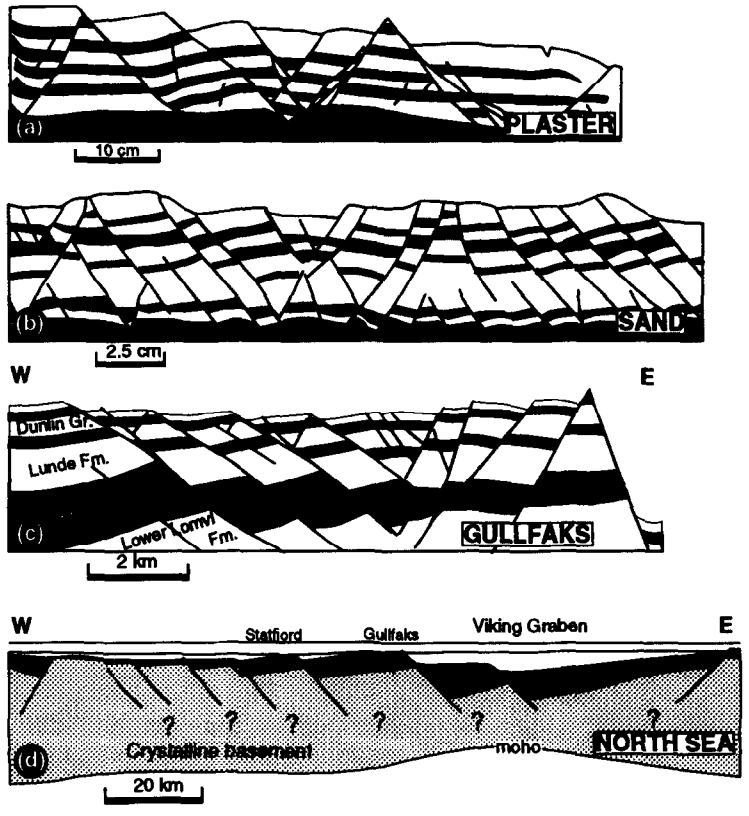

Fig. 4. Comparison of plaster experiment (a) with (b) sand-box experiment (redrawn from Vendeville *et al.* 1987, fig. 2b), (c) uneroded Gullfaks structure, northern North Sea, rotated clockwise by 5° from its present position and (d) regional profile across the North Sea as interpreted by Marsden *et al.* (1990).

Next, an antithetic normal fault system developed across block C, so that a horst was formed just to the left of the ramp. The antithetic fault separated the rotating and collapsing upper part of block C from its stable lower part, and the steep, upper part of the antithetic fault (fault 4 in Fig. 6d) became vertical and finally overturned, so that it displays an apparent reverse sense of displacement.

An important consequence of the internal deformation of block C is the progressive deformation of fault 2. Whereas the lower part of this fault became slightly steeper as it was transported down the ramp zone, its upper portion was turned into a low-angle fault as the upper part of block C rotated and collapsed. Eventually (Figs. 6d–g), fault 2 was transected and consequently offset by the antithetic fault system (fault 5).

The deformation within the horst itself appears to be mild (Fig. 6g), and the horst has maintained an unfaulted and relatively horizontal internal 'layering'. However, intense deformation is observed within the rotated block C between the horst and the listric bounding fault, with fracture density increasing towards the horst defined by fault 2 and 4 (Figs. 6g and 5a). Minor reverse faults associated with fault 2 to the right of the horst (Fig. 5a) are related to local compression during the development of the ramp in the basement.

Observations—Run 2

The basement (wet barite) was made softer than in run 1, and thus deformed passively along with the plaster without the development of a ramp or basal detachment zone. The first portion of extension is taken up in the right-hand side of the experiment. This extension is expressed by the early development of a gently right-dipping surface slope and the formation of a number of small faults on this side, in addition to a thinning of the basement (Figs. 7a & b). A slightly asymmetric graben system then developed in the central part ($\beta = 1.14$). The graben is widened by the formation of an additional master fault on either side of the graben, and the main architecture of the graben system is established after an extension of about 20–25% (Fig. 7e).

From this point on, the left-hand side of the graben is more or less unaffected by the deformation, except for continued slip along fault 1. The extension is thus accommodated by collapse of the right margin of the graben, which in particular leads to extensive internal deformation of block D (Fig. 5b). Of special interest is a zone of small, parallel faults that develop within block D (Figs. 7f–h). This zone, running from the upper left part of the block and down towards the lower right corner is interpreted as a simple shear zone in which much of the shear deformation has been taken up by a series of faults that are oriented antithetic to the zone (Fig. 8). Particle path analysis (Fig. 8b) within and around the shear zone indicates that the shear strain varies from zero at the boundaries of the shear zone to about 0.6 in the central part.

Once a fault is formed that intersects the 'layering', a point of intersection is defined which can be traced throughout the remaining deformation and hence can be

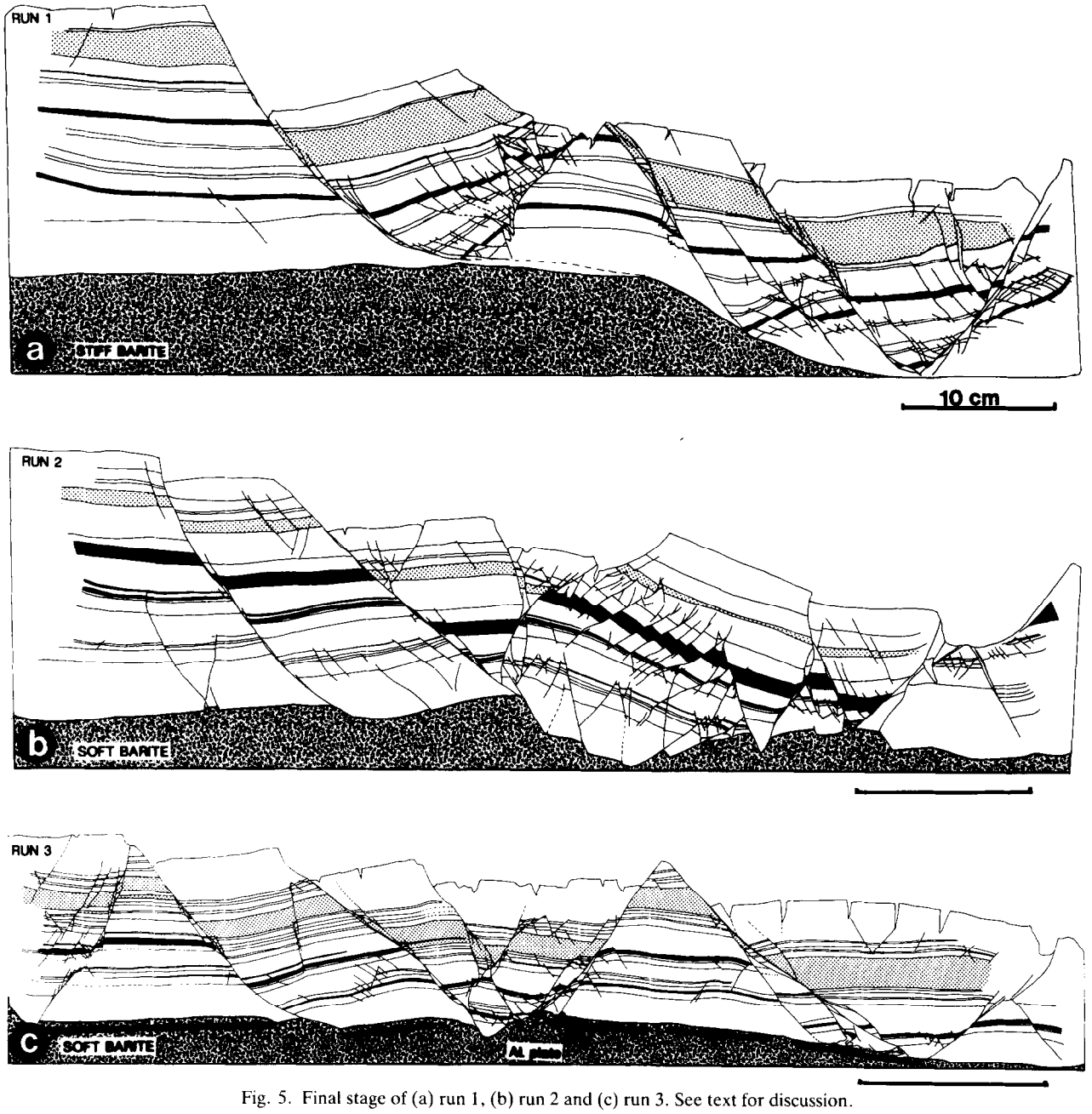

Fig. 5. Final stage of (a) run 1, (b) run 2 and (c) run 3. See text for discussion.

used to define a particle path. Clearly, both sides of an active fault (each fault block) have their individual displacement path, and in this context a fault is best considered as a surface of discontinuity in the displacement field. The displacement field has been reconstructed for run 2 (Fig. 9), and the individual paths for particles in the different blocks give the field a somewhat complex appearance. The boundary conditions of the experiments are those of pure shear, except that the upper surface is free and affected by gravitational forces rather than by a rigidly moving horizontal top. It is therefore reasonable to assume that the early stages of the experiments are dominated by this type of deformation. As the experiment proceeds and faults develop, the upper surface becomes highly irregular, and the deviations from pure shear become more marked. Nevertheless, the general particle path pattern still bears close similarities to the pure shear pattern (Fig. 9). In the case of run 2, the most significant deviations from the pure shear pattern is associated with the localized shear deformation in block D (Fig. 8), but also the major faults significantly influence on the pattern.

As in run 1, deformation of faults during the experiment is evident. This deformation is particularly well expressed by the geometric evolution of fault 2, which develops from planar (Fig. 7c) to highly curved (Z-shaped) (Fig. 7h).

Observations—Run 3

This experiment is similar to run 1, except for the five aluminum plates which were placed between the barite and the plaster (marked on Fig. 5c). The barite was made less viscous (wetter) than the first run, and approximately similar to or slightly less viscous than the second run. The aluminum plates were intended to

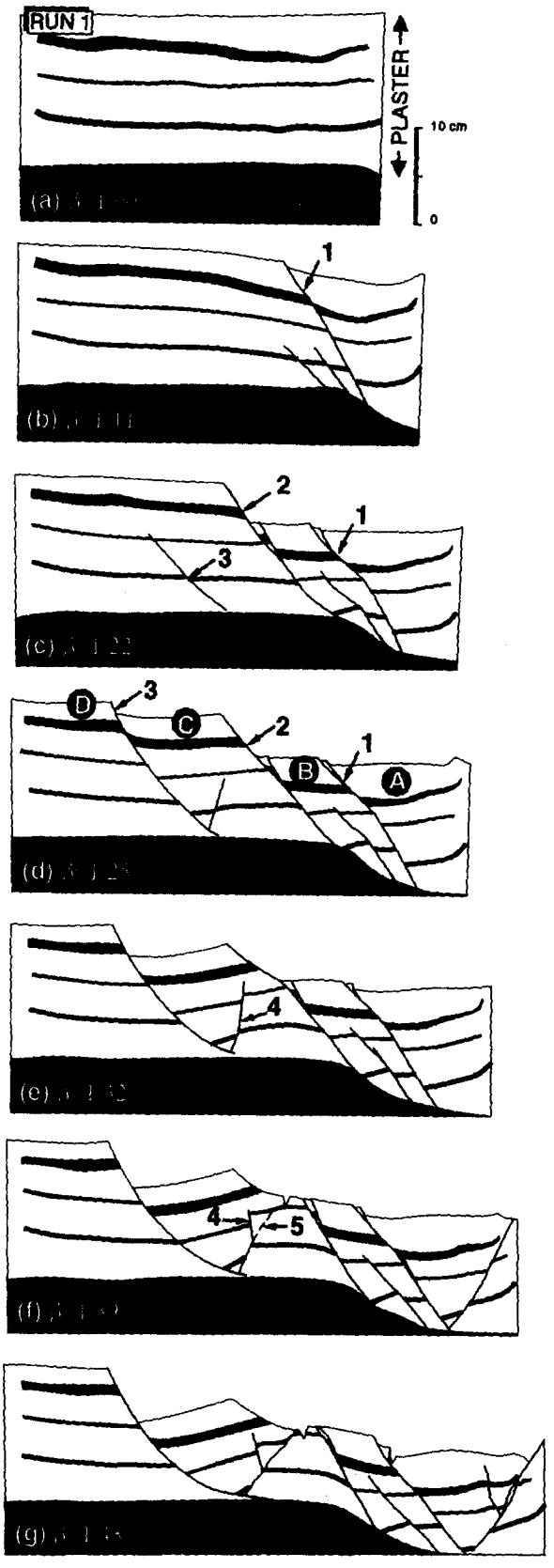

Fig. 6. Run 1, incremental stages, beginning with (a) and ending at (g). Redrawn from slide series taken during the experiment. See text for discussion.

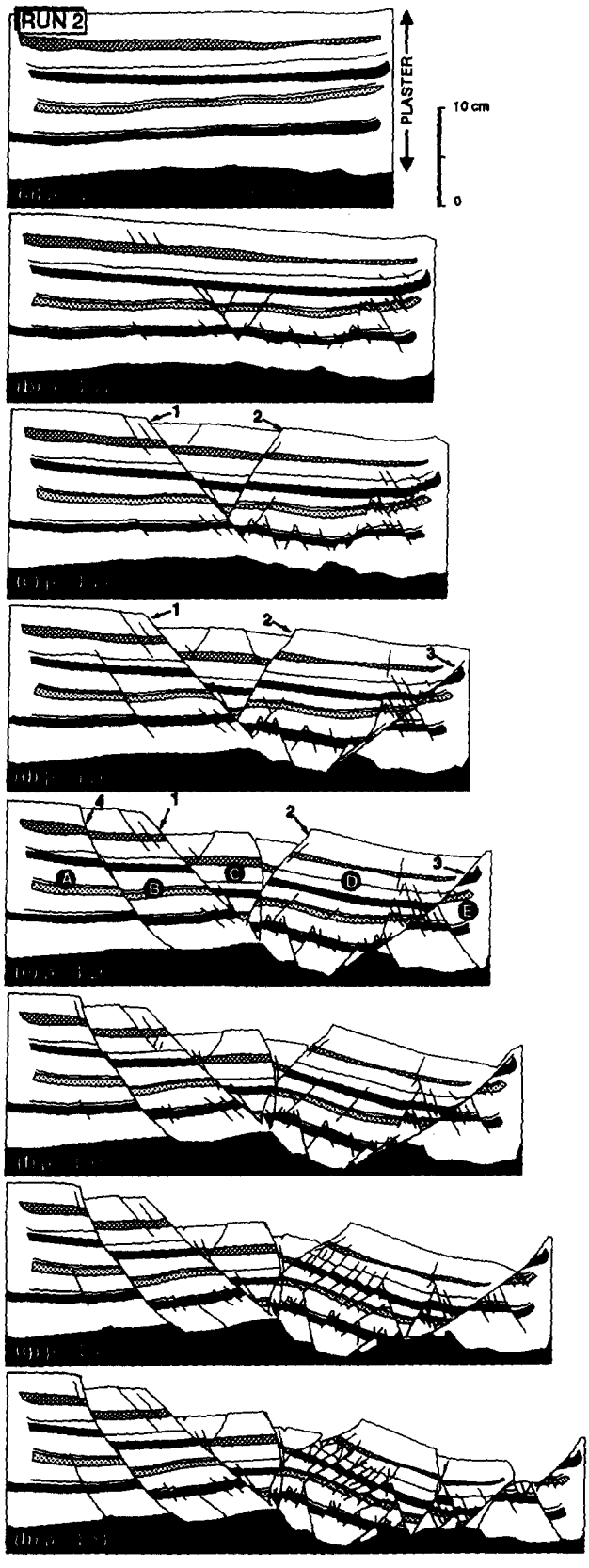

Fig. 7. Run 2, incremental stages, beginning with (a) and ending at (h). Redrawn from side series taken during the experiment. See text for discussion.

control the formation of fault blocks, and were pre-cut according to the block geometry of the Gullfaks Oilfield, northern North Sea (Fig. 4c) (Fossen & Hesthammer in press). The plates were initially separated by a few millimeters of open space, and although they apparently impose a certain control on the development of the main fault blocks, only some of the main faults form above the separations between the plates (Fig. 5c). In particular, a

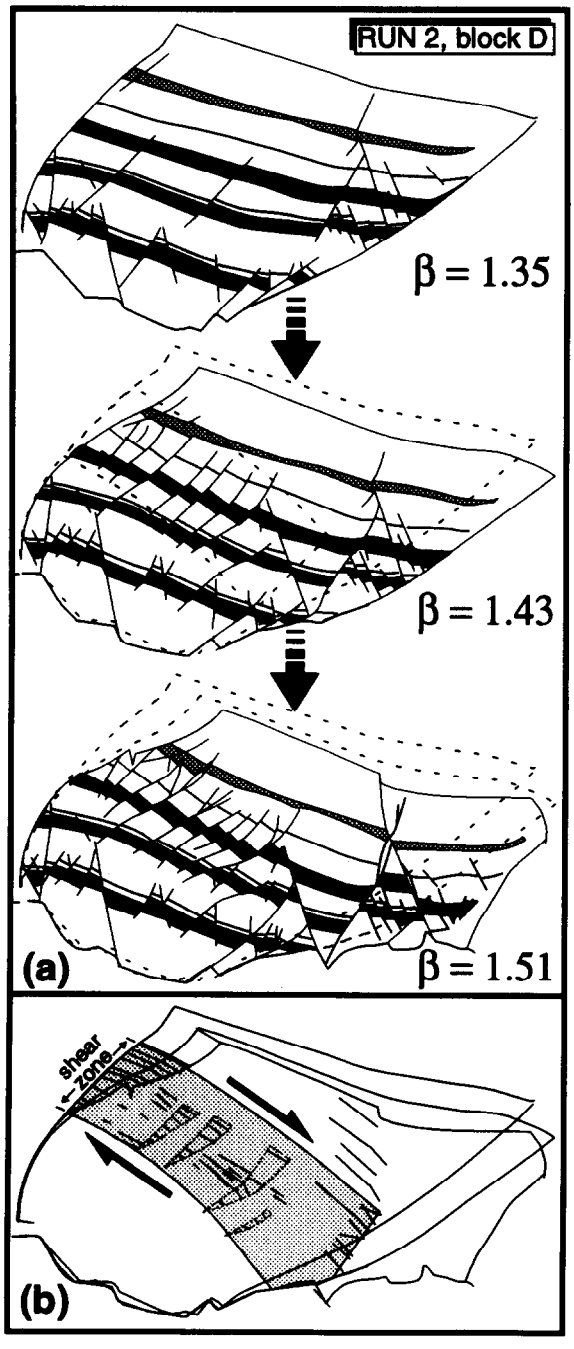

Fig. 8. (a) Block D (see Fig. 7e) during final stages of deformation, beginning with (f) and ending at (h) in Fig. 7. The block underwent a significant internal shear deformation from $\beta = 1.35$–1.51. This deformation is expressed by a right-dipping en echelon zone of almost parallel faults which subsequently become somewhat deformed (curved) by ductile deformation. The orientation and displacement pattern of the shear zone are shown in the lower figure (b). The shear strain varies from 0 to 0.6 from the margin to the core of the zone. Black lines sub-parallel to the shear zone indicate the measured particle displacement field associated with the shear zone.

dominating horst block formed above the three plates on the right-hand side of the model (block C in Fig. 10). The effect of the aluminum plates may be compared to that of strong, rigid basement blocks separated by faults and overlain by a younger sedimentary sequence. Alternatively, the setup resembles a broken sill in a sedimentary sequence.

During run 3, a graben system first developed in the right-hand side of the deformation box (Fig. 10b), defined by fault 1 and 2. Although both of these faults were active throughout the experiment, the subsequent deformation is characterized by a collapse of the footwall to fault 1 into four main blocks (blocks C–F in Fig. 10c). The general fault-block geometry was established at about 20% extension (Fig. 10c) and the collapsed footwall to fault 1 was compartmentalized into a marginal horst block (block C), similar to the horst in run 1, two blocks (E and F) bounded by right-dipping faults, and an intermediate graben system (block D).

During the last stages of deformation (Figs 10c–e), the horst (block C) remained a stable structure, whereas block E underwent counterclockwise rotation together with a small amount of internal collapse. An initially steep normal fault in block E rotated together with the rest of the block to end up as an apparent reverse fault (Figs. 5c and 10c–e), somewhat similar to fault 4 in run 1 (Figs. 6e–g). Except for its uppermost part, fault 3 shows a temporal change in geometry from convex downward to convex upward due to the gentle internal collapse of block E, again very similar to, although not as pronounced as fault 2 in run 1. Block D experienced a significant amount of stretching during the last part of the extension history, and developed a conjugate set of normal faults that operated more or less at the same time. The result is a complex series of right- and left-dipping normal faults (Fig. 5c). The rotation and collapse of block E resulted in a larger component of stretching in the upper part than the lower part of block D, and its upper part eventually ended up as a modified, gentle fold.

The main faults bordering the horst (block C) are wide fault zones, particularly in their lower part. They developed from single (narrow) fault structures to more complex and wider fault zones by propagation into the side walls. This geometry is special to run 3, and is apparently related to the presence of aluminum plates and/or to the low relief of the barite layer in this experiment (Fig. 5c). The faults nucleated within the plaster volume and grew to meet the aluminum plate in the basement. At this point new faults with slightly lower dips formed close to the old faults in the hanging wall. Together the faults form wide fault zones.

The small-scale deformation is more common in the rotated fault blocks and graben systems than in the horst structures (Fig. 5c). This feature was also observed from run 1, and cannot therefore be attributed merely to the stabilizing effect of the aluminum plates.

ANALYSIS OF RESULTS

A particular advantage of plaster experiments is the possibility of studying and comparing faults of different orders of magnitude. Several features appear to be common for the different experiments and are thus thought to have general application. One of these is the relationship between the main faults and associated minor faults, which closely resembles examples observed in the field.

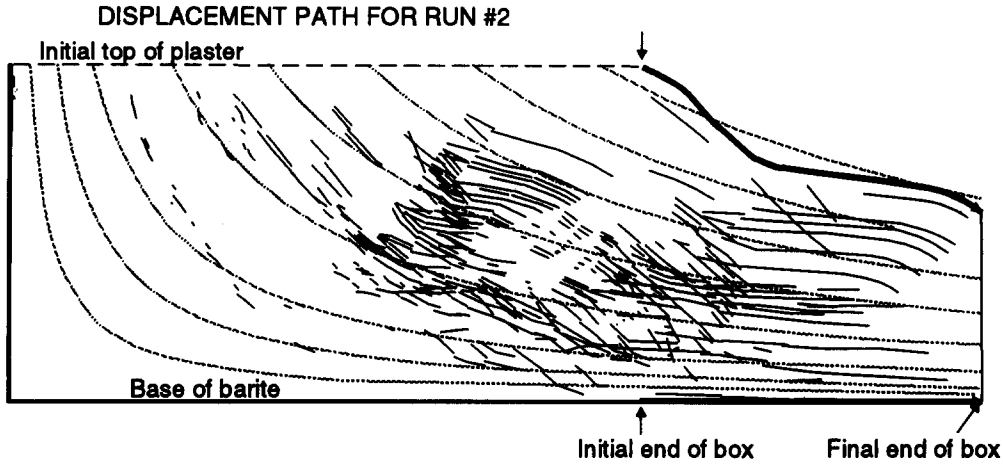

Fig. 9. (a) Total particle path for run 2. Path of first (b) and last (c) part of the deformation have the theoretical particle paths of pure shear superimposed for comparison.

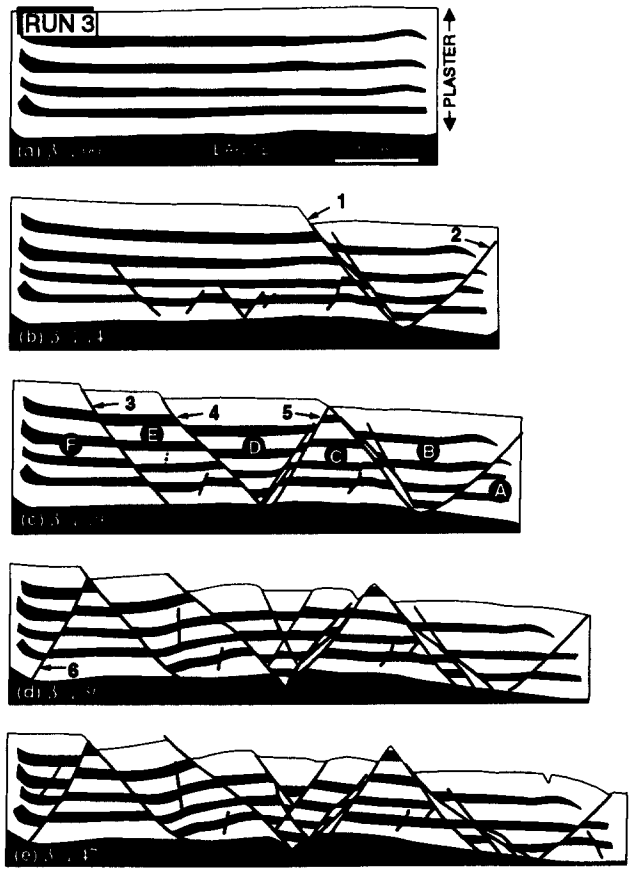

Fig. 10. Run 3, incremental stages, beginning with (a) and ending at (e). Redrawn from video recording.

Main faults and associated structures

The fault developed in the plaster experiments may be subdivided into two types: those cross-cutting the entire section and those that do not. Faults in the first category are called main faults in this paper. They appear as sharp discontinuity surfaces with associated minor faults. Minor faults that are directly linked to major faults are mostly synthetic to, and have steeper dips than, the master faults. It appears that this particular type of minor faults evolved from the master fault and grew into the hanging wall or footwall. The result is a single 'parasitic' fault or a family of such structures, commonly with a slightly listric geometry. A typical feature of these faults is their gradually decreasing displacement away from the main fault until they terminate within the footwall or hanging wall (Figs. 11a and 2b & c). The development of such parasitic faults are more common in the hanging wall than in the footwall, although both are observed. Another characteristic feature is the formation of isolated lenses along the main fault (Fig. 11b), i.e. a type of extensional duplexes as defined by Gibbs (1984) (see also Wernicke 1981). These two types of structures (parasitic and anastomosing structures) may coexist in the plaster experiments, as seen in Fig. 2(b), and represent different ways of forming so-called

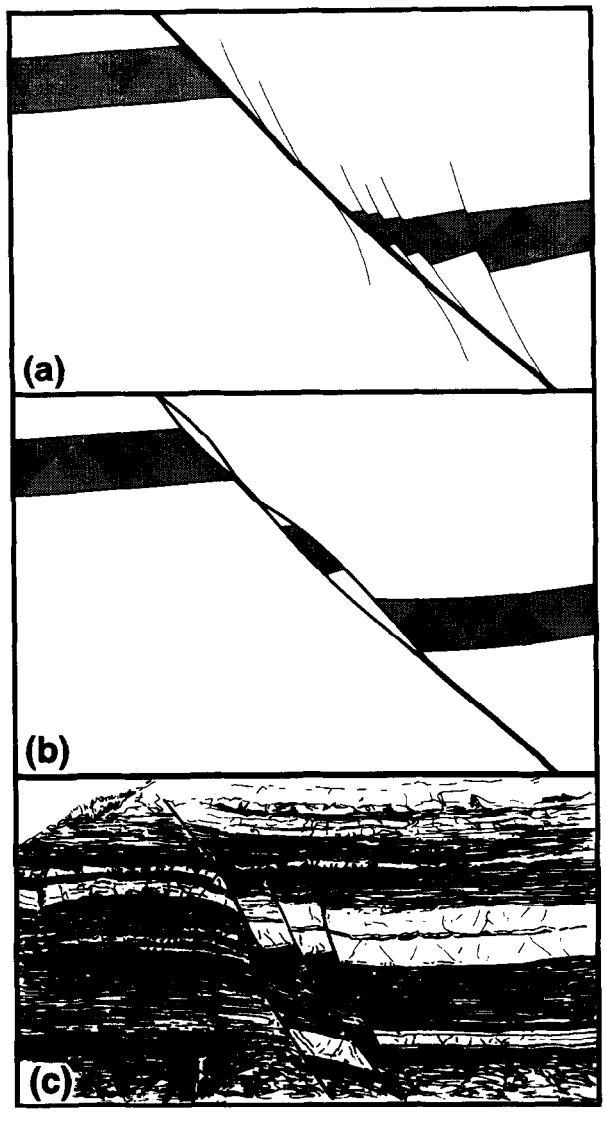

Fig. 11. Diagram of two common types of fault complexities along main faults as observed in the plaster models: (a) minor faults connected to the main fault that die out into the hanging wall/footwall; (b) lensoid geometry along the main fault zone. (c) Field example of the geometries illustrated in (a) and (b). The main fault that runs down to the right splays into two faults to define the upper part of a tectonic lens. Two minor faults emerge from the main fault and die out upwards into the hanging wall to the right. Railroad cut through the Green River Formation 3 km west of Skyview near Tucker, Utah.

damage zones around main faults. Similar structures are found in the field (Fig. 11c).

Collapse of the upper part of footwalls to major faults was observed (fault 2 in Figs. 6d–f, and fault 2 in Figs. 7f–h). The result is a pronounced change in fault geometry from initially (sub)planar to strongly non-planar shapes. The fault retains its steep dip at depth, and, to some extent, also in its uppermost part, but most of the upper part of the fault experiences progressive flattening. This development is commonly observed in plaster experiments (Sales personal communication).

Geometrically, the fault development observed in the plaster models is similar to that suggested by Wernicke & Axen (1988) for faults in the Basin and Range province, and to the fault development modeled numerically by Buck (1988). In all cases, the rotating upper part of the fault eventually becomes horizontal. However, the models suggested by Buck (1988) and Wernicke & Axen (1988) involve isostasy at the scale of the entire crust, whereas the plaster experiments describes gravitational collapse above a fixed base and is therefore more applicable to upper crustal sections. Such upper crustal footwall collapse is interpreted from the northern North Sea (Graue 1992), and the plaster example represents a model for the formation of such curved, low-angle upper crustal fault geometries.

Internal block deformation

In addition to the extension accommodated by the main faults, a certain amount is taken up by deformation *within* the fault blocks. Internal block deformation includes both minor faults and smaller-scale, ductile deformation. Small, visible faults make a significant contribution, e.g. during deformation of block D in run 2 (Fig. 8). However, the changes in geometry of some of the blocks appear to require additional micro-scale ('ductile') deformation.

As expected, minor faults appear to be more common in rotated blocks, in low graben blocks and in zones where they obviously help accommodate abrupt geometric changes, e.g. in block C, run 2. The flanking blocks as well as the horsts are, however, less affected by internal faulting.

Internal block deformation can generally be demonstrated by comparing the rotation of the layering and the main faults. If the fault blocks rotate rigidly, the layering and the main faults maintain their initial angular relationship. This angular relationship is the basic assumption used by some authors for reconstructing initial fault dips (e.g. Jackson 1987). However, since deformation is expressed at a wide range of scales, internal block deformation will almost always be a factor to consider. The difference in rotation between the layering and the block-bounding faults (called 'tilt discrepancy' by Westaway & Kusznir 1993) is thus a measure of the block-internal or distributed deformation. Consequently, the angle between the fault and the layering remains fixed for rigid-body rotations, whereas if it changes, there has to be some additional internal block deformation. Plotting this angle for fault 2, run 2 (Fig. 12), shows that the fault and the layering rotate by different amounts, proving the presence of significant block-internal deformation in the plaster experiments. The actual amount of internal deformation can not be extracted from data such as the angular relationship between layering and faults alone, but depend on the type of internal deformation. A distributed vertical simple shear would, for example, be more efficient in changing the angle between the layering and a fault than would an inclined shear deformation. In fact, the nature of block-internal deformation has been a topic of major concern, and proposed models involve distributed vertical shear (Verrall 1981, Gibbs 1983, Westaway & Kusznir 1993), oblique shear (White *et al.* 1986) and bedding-parallel slip (Higgs *et al.* 1991). In addition, some authors still

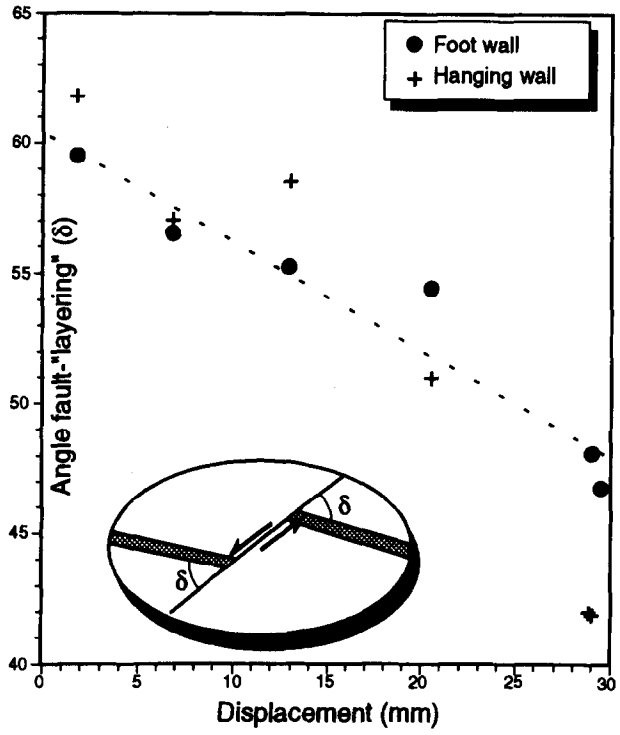

Fig. 12. Angle between fault 3, run 2 (see Fig. 7e) and the adjacent layering, plotted against the displacement recorded along the fault during the run. The decrease in angle on both sides of the fault during deformation strongly indicates the presence of ductile block-internal deformation in both the hanging wall and the footwall.

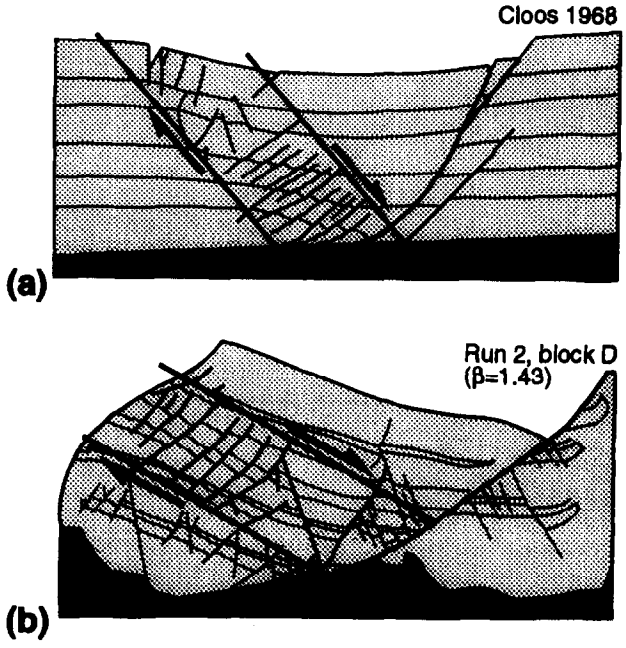

Fig. 13. (a) Illustration of the clay experiment performed by Cloos (1968), where an en echelon zone of synthetic faults developed antithetically to the main fault. (b) Shows the similarities to the en echelon fault system of minor faults in block D, run 2.

favor the domino or rigid-body rotation model, where internal deformation is absent or negligible (e.g. Jackson 1987, Jackson *et al.* 1988, Moretti & Colletta 1988).

As demonstrated above (e.g. Fig. 12), evidence is compelling that rigid-body rotation alone fails to explain the observations made from the plaster experiments. If the fault blocks deformed by vertical shear, then no faults could possibly rotate through the vertical plane (i.e. the shear plane). However, the steep normal fault in run 1 obviously rotates to become an apparent reverse fault, and a similar rotation history is recorded in run 3 (steep fault in block E, Fig. 10). Hence, the vertical shear model can not explain all of the internal ductile block deformation.

Bedding-plane slip (shear) clearly does not operate in the plaster experiments, since no mechanical layering is present. Hence, we are left with inclined shear as the only simple explanation. This explanation is in accordance with observations by Ellis & McClay (1988), who estimated that the shear angle was antithetic to the main fault, and varied spatially and temporally from 10° to 80° in a single fault block. Oblique block-internal shear is also demonstrably present in block D of run 2 (Fig. 8). This sort of localized block-deformation implies a shear antithetic to the master fault, but the visual expression of this deformation is an en echelon arranged zone of synthetic faults. This expression is in fact very similar to the deformation structures developed in the hanging wall to a major fault in the clay model of Cloos (1968) (see Fig. 13). If the experimental medium had anisotropic properties across the layering (as in most natural stratigraphic sequences), it is likely that the deformation shown in Figs. 8 and 13(b) would have been accommodated by bedding-parallel slip or shear.

Strain estimates and displacement distributions

Recent advances in structural geology indicate that several attributes of natural fault populations follow a power-law distribution, i.e.

$$N = bS^{-D},$$

where S is a linear size attribute such as displacement, D reflects the fractal dimension or the slope of the line, b is a constant and N (cumulative frequency) is the number of faults with size equal to or larger than S (e.g. Hirata 1989, Kojima *et al.* 1989, Childs *et al.* 1990, Walsh *et al.* 1991, Marrett & Allmendinger 1992, Gauthier & Lake 1993, Peacock & Sanderson 1994).

Maximum displacement was measured on the entire visible fault population in the three plaster models. The results (Fig. 14) show a roughly straight line segment with slope about −1.0 or slightly less, indicating that the fault population has a power-law distribution of displacement in this range. Together with the gently sloping left-hand segment that represents data below the limit of general resolution, the pattern is very similar to naturally formed fault populations as reported by various authors during the last decade (e.g. Marrett & Allmendinger 1992, Walsh & Watterson 1992). The D-exponents for the three fault populations are all quite similar (Fig. 14), indicating that the relative number of small and large faults are not very different for the different models.

The plaster models were subjected to total horizontal extensions of 48, 51 and 47%, respectively. It is interest-

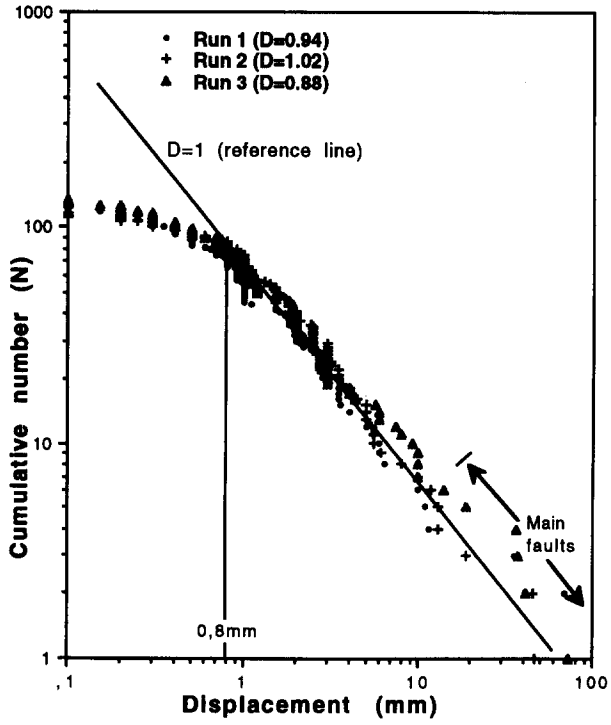

Fig. 14. Cumulative frequency (N) plotted against maximum displacement of minor faults in a log–log plot for the three runs. A straight segment through most of the data may indicate a fractal displacement distribution. A break in slope occurs at about 0.8 mm, corresponding to the resolution of the data. See text for discussion.

ing to compare the total extension of each run with the contribution from main faults, minor faults and deformation below resolution (ductile deformation). Constant bed-length balancing shows that the main, cross-cutting faults account for *ca* 63% (run 1), 69% (run 2) and 60% (run 3) of the total extension, whereas the corresponding numbers for smaller, block-internal faults are about 17, 12 and 12%, respectively. The remaining extension, i.e. 20% for run 1, 19% for run 2 and 28% for run 3, must therefore be taken up by smaller-scale deformation. We know that about 5–10% of this extension is accommodated by ductile stretching prior to faulting, hence the remaining 10–18% is ductile deformation that must have occurred during the faulting history.

The break in slope at around 0.8 mm displacement in Fig. 14 is thought to coincide with the visual resolution of the collected data. Faults with throw less than 0.8 mm are incompletely sampled, resulting in a degraded curve for faults with displacement less than 0.8 mm. This break is similar to the one seen on data from seismic interpretations, where it generally coincides with the resolution of the seismic data. We can thereby conclude that 10–18% of the syn-faulting extension and 20–28% of the total extension is recorded by deformation at a scale below data resolution. According to the experimental scaling factor mentioned above, 0.8 mm corresponds to faults with maximum displacement on the order of 8–80 m in the field, i.e. roughly equal to the resolution of commercial seismic data from the North Sea and similar areas. Some fault models suggest that a significant amount (up to 60% in the North Sea) of the extension is accommodated by small-scale (sub-seismic) deformation (Walsh *et al.* 1991, Marrett & Allmendinger 1992). If the plaster results are representative for natural fault populations, they may support the view that sub-seismic faults only accommodate a minor portion of the total extension, as advocated by Scholtz & Cowie (1990) and Westaway (1994).

DISCUSSION AND CONCLUSION

Detailed analysis of the three plaster models shows how extensional structures very similar to those observed in naturally deformed rocks may be reproduced in the laboratory at a smaller scale. Systems of fault blocks formed under plane-strain extensional deformation of barite and plaster mimic published cross-sections from the North Sea and other extensional basins, and may give additional information or new ideas as to their temporal development and structural details.

The experiments show that major faults are composite features which vary along dip from single faults to complex fault zones. Two categories of fault morphologies are identified: (1) lense-shaped geometries; and (2) associated small synthetic faults dipping more steeply than the main zone. In general, the main displacement tends to be taken up along a single fault surface, whereas associated faults have smaller offsets.

Internal deformation in the blocks between the main fault zones occurs as: (a) scattered faults with small displacements that are not obviously associated with any other structure; (b) single or almost single fault structures associated with the geometry of a larger, underlying fault, e.g. antithetic faults associated with a bend in the main fault; and (c) zones or swarms of normal faults accommodating significant internal shear deformation of a collapsing fault block, e.g. internal shear across the block. Scattered faults (a) are characteristic of footwall deformation, whereas single faults (b) and zones of faults (c) occur in the hanging wall to major fault zones. The distribution of fault displacements closely follows a power law in the range of 0.8–80 mm of displacement for all of the plaster models, similar to natural fault populations. The extension accommodated by ductile (sub-resolution) extension is estimated to less than 20–30% for all three examples, whereas the main, through-cutting faults accommodate 60–70% of the total extension. This supports the view that the majority of the extension is taken up by larger faults, and that the role of 'sub-seismic' faults in contributing to the total strain in areas of plane-strain extension is relatively small.

It is demonstrated that steep, apparently reverse faults may form by passive rotation of steep normal faults. This rotation typically occurs in the hanging wall of non-planar faults, which demonstrates that internal block deformation cannot be explained by vertical shear alone.

Collapse of the upper part of fault blocks (footwalls to

major faults) which results in strongly curved fault planes and a low-angle, upper part of the fault occurred. This development describes a model for footwall collapse in the middle to upper crust.

Acknowledgements—The authors wish to thank John Sales for introducing one of us (R. H. Gabrielsen) to the technique of plaster modeling. R. Færseth, P. Haremo, J. Korstgård and A. G. Milnes are thanked for reading an early version of this manuscript. Reviews by W. J. Taylor and J. P. Evans lead to valuable improvements of the text.

REFERENCES

Braun, J., Batt, G. E., Scott, D. L., McQueen, H. & Beasley, A. R. 1994. A simple kinematic model for crustal deformation along two- and three-dimensional listric normal faults derived from scaled laboratory experiments. *J. Struct. Geol.* **16**, 1477–1490.

Brun, J. P., Sokoutis, D. & Driessche, J. V. D. 1994. Analogue modeling of detachment fault systems and core complexes. *Geology* **22**, 319–322.

Buck, W. R. 1988. Flexural rotation of normal faults. *Tectonics* **7**, 959–973.

Byerlee, J. D. 1978. Friction of rocks. *Pure & Appl. Geophys.* **116**, 615–626.

Cadel, H. M. 1890. Experimental researches in mountain building. *Trans. R. Soc. Edinb.* **35**, 337.

Childs, C., Walsh, J. J. & Watterson, J. 1990. A method for estimation of the density of fault displacements below the limits of seismic resolution in reservoir formations. In: *North Sea Oil and Gas Reservoirs—II* (edited by Buller, A. T., Berg, E., Hjelmeland, O., Kleppe, J., Torsæter, O. & Aasen, J. O.). Graham & Trotman, London, 309–318.

Cloos, E. 1955. Experimental analysis of fracture patterns. *Bull. geol. Soc. Am.* **66**, 241–256.

Cloos, E. 1968. Experimental analysis of Gulf Coast fracture patterns. *Bull. Am. Ass. Petrol. Geol.* **52**, 420–441.

Cloos, H. 1929. Künstliche Gebirge. *Natur. Museum* **5**, 225–243.

Cloos. H. 1930. Zur experimentellen Tektonik. Methodik und Beispiele. *Naturwissenschaften* **18**, 741–747.

Cloos, H. 1931. Zur experimentellen Tektonik. Brüche und Falten. *Naturwissenschaften* **19**, 242–247.

Ellis, P. G. & McClay, K. R. 1988. Listric extensional fault systems — results of analogue model experiments. *Basin Res.* **1**, 55–70.

Fossen, H. & Hesthammer, J. In press. Structural geology of the Gullfaks Field, northern North Sea. In: *Structural Geology in Reservoir Characterization and Field Development* (edited by Coward, M. P.). *Spec. Pub. geol. Soc. Lond.*

Gabrielsen, R. H., Grunnaleite, I. & Ottesen, S. 1992. Reactivation of fault complexes in the Loppa High area, southwestern Barents Sea. In: *Arctic Geology and Petroleum Potential* (edited by Vorren, T. O., Bergsager, E., Dahl-Stamnes, Ø. A., Holter, E., Johansen, B., Lie, E. & Lund, T. B.). *Spec. Publ. Norweg. Petrol. Soc.* **2**, 631–641.

Gauthier, B. D. M. & Lake, S. D. 1993. Probabilistic modeling of faults below the limit of seismic resolution in Pelican Field, North Sea, offshore United Kingdom. *Bull. Am. Ass. Petrol. Geol.* **77**, 761–777.

Gibbs, A. D. 1983. Balanced cross-section construction from seismic sections in areas of extensional tectonics. *J. Struct. Geol.* **5**, 153–160.

Gibbs, A. D. 1984. Structural evolution of extensional basin margins. *J. geol. Soc. Lond.* **141**, 609–620.

Graue, K. 1992. Extensional tectonics in the northernmost North Sea: rifting, uplift, erosion and footwall collapse in Late Jurassic to Early Cretaceous times. In: *Generation Accumulation and Production of Europe's Hydrocarbons—II* (edited by Spencer, A. M.). Springer, Berlin, 23–34.

Grunnaleite, I. 1991. En tektonisk/kinematisk analyse av Bjørnøyrenneforkastningskomplekset, SV-Barentshavet, med spesiell vekt på den krittassiske og tertiære utviklingen. Unpublished Cand. scient. thesis, University of Bergen.

Higgs, W. G., Williams, G. D. & Powell, C. M. 1991. Evidence for flexural shear folding associated with extensional faults. *Bull. geol. Soc. Am.* **103**, 710–717.

Hirata, T. 1989. Fractal dimension of fault systems in Japan: fractal structure in rock fracture geometry at various scales. *Pure & Appl. Geophys.* **131**, 157–170.

Horsfield, W. T. 1977. An experimental approach to basement-controlled faulting. *Geologie Mijnb.* **56**, 363–370.

Horsfield, W. T. 1980. Contemporaneous movement along crossing conjugate normal faults. *J. Struct. Geol.* **2**, 305–310.

Hubbert, M. K. 1937. Theory of scale models as applied to geologic structures. *Bull. geol. Soc. Am.* **48**, 1459–1520.

Jackson, J. A. 1987. Active normal faults and crustal extension. In: *Continental Extensional Tectonics* (edited by Coward, M. P., Dewey, J. F. & Hancock, P. L.). *Spec. Pub. geol. Soc. Lond.* **28**, 3–17.

Jackson, J. A., White, N. J., Garfunkel, Z. & Anderson, H. 1988. Relations between normal-fault geometry, tilting and vertical motions in extensional terrains: an example from the southern Gulf of Suez. *J. Struct. Geol.* **10**, 155–170.

Kojima, K., Toaska, H. & Ohno, H. 1989. An approach to wide-ranging correlation of fracture distributions using the concept of fractal. In: *Rock Mechanics as a Guide for Efficient Utilization of Natural Resources* (edited by Khair). Balkema, Rotterdam, 211–218.

Mandl, G. 1988. *Mechanics of Tectonic Faulting. Models and Basic Concepts.* Elsevier, Amsterdam.

Marsden, G., Yielding, G., Roberts, A. M. & Kusznir, N. J. 1990. Application of a flexural cantilever simple-shear/pure-shear model of continental lithosphere extension to the formation of the northern North Sea Basin. In: *Tectonic Evolution of the North Sea Rifts* (edited by Blundell, D. J. & Gibbs, A. D.). Oxford University Press, Oxford, 240–261.

Marrett, R. & Allmendinger, R. W. 1992. Amount of extension on "small" faults: an example from the Viking Graben. *Geology* **20**, 47–50.

McClay, K. R. 1990. Extensional fault systems in sedimentary basins: a review of analogue model studies. *Mar. Petrol. Geol.* **7**, 206–233.

McClay, K. R. & Ellis, P. G. 1987a. Analogue models of extensional fault geometries. In: *Continental Extensional Tectonics* (edited by Coward, M. P., Dewey, J. F. & Hancock, P. L.). *Spec. Publs geol. Soc. Lond.* **28**, 109–125.

McClay, K. R. & Ellis, K. R. 1987b. Geometries of extensional fault systems developed in model experiments. *Geology* **15**, 341–344.

Moretti, I. & Colletta, B. 1988. Fault-block tilting: the Gebel Zeit example. Gulf of Suez. *J. Struct. Geol.* **10**, 9–19.

Naylor, M. A., Mandl, G. & Sijpesteijn, C. H. K. 1986. Fault geometries in basement-induced wrench faulting under different initial stress states. *J. Struct. Geol.* **8**, 737–752.

Odinsen, T. 1992. *Modellering av normalforkastninger: analoge ekstensjons-gipsmodeller og balansering.* Unpublished Cand. scient thesis, University of Bergen.

Oertel, G. 1962. Stress, strain and fracture in clay models of geologic deformation. *Geotimes* **6**, 26–31.

Oertel, G. 1965. The mechanism of faulting in clay experiments. *Tectonophysics* **2**, 343–393.

Ottesen, S. 1991. Den strukturelle utviklingen av Swaengraben, og dens implikasjoner for strukturering av Lopphøgda med omgivelser. Unpublished Cand. scient. thesis, University of Bergen.

Peacock, D. C. P. & Sanderson, D. J. 1994. Strain and scaling of faults in the chalk at Flamborough Head, U.K. *J. Struct. Geol.* **16**, 97–107.

Ramberg, H. 1981. *Gravity, Deformation and the Earth's Crust as Studied by Centrifugal Models* (2nd edn). Academic Press, New York.

Rettger, R. E. 1935. Experiments in soft rock deformation. *Bull. Am. Ass. Petrol. Geol.* **19**, 271–292.

Sales, J. K. 1987. Tectonic models. In: *Encyclopedia of Structural Geology and Tectonics* (edited by Seyfert, C. K.). Van Nostrand Reinhold, New York, 785–794.

Scholz, C. H. & Cowie, P. A. 1990. Determination of total strain from faulting using slip measurements. *Nature* **356**, 837–839.

Tchalenko, J. S. 1970. Similarities between shear zones of different magnitudes. *Bull. geol. Soc. Am.* **81**, 1625–1640.

Vendeville, B., Cobbold, P. R., Davy, P., Brun, J. P. & Choukroune, P. 1987. Physical models of extensional tectonics at various scales. In: *Continental Extensional Tectonics* (edited by Coward, M. P., Dewey, J. F. & Hancock, P. L.). *Spec. Pub. geol. Soc. Lond.* **28**, 95–107.

Verrall, P. 1981. Structural interpretation with application to North Sea problems. Course Notes No. 3. Joint Association for Petroleum Exploration Courses. London, U.K.

Walsh, J. J. & Watterson, J. 1988. Dips of normal faults in British coal measures and other sedimentary sequences. *J. geol. Soc. Lond.* **145**, 859–873.

Walsh, J. J. & Watterson, J. 1992. Populations of faults and fault displacements and their effects on estimates of fault-related regional extension. *J. Struct. Geol.* **14**, 701–712.

Walsh, J., Watterson, J. & Yielding, G. 1991. The importance of small-scale faulting in regional extension. *Nature* **351**, 391–93.

Wernicke, B. 1981. Low-angle normal faults in the Basin and Range Province: nappe tectonics in an extending orogen. *Nature* **291**, 645–648.

Wernicke, B. & Axen, G. J. 1988. On the role of isostasy in the evolution of normal fault systems. *Geology* **16**, 848–851.

Westaway, R. 1994. Quantitative analysis of populations of small faults. *J. Struct. Geol.* **16**, 1259–1273.

Westaway, R. & Kusznir, N. 1993. Fault and bed 'rotation' during continental extension: block rotation or vertical shear? *J. Struct. Geol.* **15**, 753–770.

White, N. J., Jackson, J. A. & McKenzie, D. P. 1986. The relationship between the geometry of normal faults and that of the sedimentary layers in the hanging walls. *J. Struct. Geol.* **8**, 897–909.

Withjack, M. O., Islam, Q. T. & La Pointe, P. R. 1995. Normal faults and their hanging-wall deformation: an experimental study. *Bull. Am. Ass. Petrol. Geol.* **79**, 1–18.